Polymer 50 (2009) 860–871

Contents lists available at ScienceDirect

Polymer

journal homepage: www.elsevier.com/locate/polymer

Well-defined silica core–poly(vinyl pyrrolidone) shell nanoparticles: Interactions and multi-modal glass transition dynamics at interfaces

Vladimir Bershtein [a,*], Vladimir Gun'ko [b], Larisa Egorova [a], Natalia Guzenko [b], Eugene Pakhlov [b], Valery Ryzhov [a], Vladimir Zarko [b]

[a] Materials Dynamics Laboratory, Ioffe Physico-Technical Institute RAS, Department of Solid State Physics, 26 Polytekhnicheskaya Str., 194021 St. Petersburg, Russia
[b] Department of Amorphous and Structurally Ordered Oxides, Institute of Surface Chemistry NAS, 03164 Kiev, Ukraine

ARTICLE INFO

Article history:
Received 8 September 2008
Received in revised form
14 November 2008
Accepted 5 December 2008
Available online 24 December 2008

Keywords:
Core–shell particles
Interfacial interactions
Dynamics

ABSTRACT

Interfacial interactions/dynamics were studied in silica core–poly(vinyl pyrrolidone) (PVP) shell nanoparticles with the shell thickness of 1–2 (monolayer), 2–5, 5–15, and 8–25 nm using far- and mid-IR spectroscopy and DSC activation analysis of the glass transition. Particles were prepared using a pseudo-liquid state procedure. Their geometry, structural organization and shell uniformity were characterized comprehensively by LTNA, AFM, QELS, FT-IR and densitometry techniques. As revealed, strong core–shell interfacial interactions, including hydrogen bonding and Lewis acid–base ones, resulted in the quite different, multi-modal glass transition dynamics in PVP nano shells. For 1–2 nm thick monomolecular PVP shell, only several "abnormal" modes, including constrained cooperative and non-cooperative as well as ultra-fast non-cooperative ones, constituted segmental dynamics in the glass transition; the latter covered the range from 70 to 230 °C, with varying apparent activation energy by one order of magnitude. Ultra-fast dynamic mode was caused by collapse of motional cooperativity (α- to β-relaxation transformation).

1. Introduction

Starting from the pioneer works [1–4], a large series of the experimental studies of dynamics for polymers in ultrathin films, adsorbed on solid substrates or in free-standing state, and in nanovolumes of polymer nanocomposites (mostly with 2D silicate nanolayers) have been performed [1–26]. In these studies, reviewed particular in [6,18,19], it was shown that glass transition dynamics under these conditions may dramatically differ from that in a bulk polymer as a result of nanoscale confinement, with or without strong interaction of confined substance with the restricting surface, or location of chains at free (polymer–air) surface.

Slowing down segmental dynamics with increasing T_g [3,10,15,24] or, contrarily, T_g reduction (accelerating dynamics) in polymer nanolayers were observed [2,5,7,12,13,20]. As De Gennes indicated [17], "future experiments should aim not at the determination of a single T_g but a distribution of T_gs in thin polymer films". Really, a co-existence of both anomalously fast and ultra-slow segmental dynamics modes in the glass transition could sometimes be observed [6,11,14,16,25,26]. Two glass transitions or anomalously shifted glass transition were observed in polymer–silica nanocomposites [27–30]. Manias and Torkelson with co-workers published the first MD simulations/NMR [12,14] and fluorescence data [16] demonstrating the distribution of T_gs across polymer film of several tens of nanometers in thickness [16], or a very wide distribution of segmental relaxation times in polymer confined in 1–2 nm wide slits (polymer-layered silicate nanocomposite) [14]. The numerous studies of peculiar glass transition dynamics in complex polymer systems have also been performed for last twenty years, starting probably from the works on block copolymers [31–33] and graft copolymers [33,34]. Similarly, the opposite effects of slowing down/acceleration of dynamics, compared to that in neat polymers, have been shown (see e.g. reviews [33,35]). These results were interpreted proceeding from the notions of constrained dynamics, dynamics in nanoscale confinement, and of the common segmental nature of α - and β - relaxations (see below).

In the studies of ultrathin films adsorbed on solid surface, using computer simulations [36–38], FT-IR spectroscopy [39], and small-angle neutron scattering (SANS) [40] techniques, it was found that the strongly adsorbed chains acquired the quasi-2D (flattened, "pancake") conformations instead of 3D conformations peculiar to bulk polymer. Day and Robb [41] studied by FT-IR spectroscopy PVP

* Corresponding author. Tel.: +7 812 2927172; fax: +7 812 2971017.
E-mail address: vbersht@polmater.ioffe.ru (V. Bershtein).

0032-3861/$ – see front matter © 2008 Elsevier Ltd. All rights reserved.
doi:10.1016/j.polymer.2008.12.024

adsorbed on silica and confirmed that, indeed, initially the PVP molecules were adsorbed onto silica in a flat configuration ("trains" formation from segments bound by the hydrogen bonds with silica surface), but at a higher surface coverage adsorbed nanolayers had more chain loops and tails.

Thus, a significant amount of work has already been done to date on peculiar dynamics in thin polymer films on solid substrates or confined in nanovolumes. Nevertheless, much experimental research still remains to be done, especially in order to trace the direct connections between the interfacial interactions, conformation state of macromolecules at interfaces and peculiar polymer dynamics within interfacial 1–2 nm thick polymer monolayer. Solving this problem may be considered as one of the cardinal tasks for the development of high performance polymer nanocomposites, adhesives, coatings, as well as inorganic core–polymer shell nanoparticles.

Nanooxides are used in industrial and medicinal materials as powders or compact solids, fillers of polymer materials, or as cores in core–polymer shell nanoparticles [42–46]. Nanooxide core–polymer shell nanoparticles, besides their applied significance, are of large interest as "interface-controlled materials" and good model systems for studying the interactions and dynamics at polymer–substrate interfaces, over the distances ranging from the statistical segment length (typically of 1.5–3 nm for flexible-chain polymers) to the radius of gyration R_g of macromolecule. Fumed silica nanoparticles covered with hydrophilic polymers, such as poly(vinyl pyrrolidone) (PVP), poly(ethylene glycol) or poly(vinyl alcohol), are of interest for applications in medicine, biotechnology, and biochemistry [46,47]. These core–shell particles may represent very loose materials (bulk density $\rho_b \sim 0.04$–0.13 g/cm^3) and form aggregates ($\ll 1$ μm in size, mass fractal dimension $D_{mf} = 2.5$–2.6, density $\rho_b \approx 0.3\rho_0$ where ρ_0 is the true density of non-porous sample), and agglomerates of aggregates (>1 μm in size, $D_{mf} = 2.2$–2.3, $\rho_b \approx 0.04\rho_0$). A number of factors affect the packing of primary particles into secondary structures [42–51].

Previously [52–54], a set of silica core–PVP shell nanoparticles were prepared and characterized by different techniques (LTNA, QELS, FT-IR, AFM, modeling). In this paper, we only very briefly report some of these results obtained for particles under study, and then present the new results of the analysis of interfacial interactions and the dynamics of PVP shells. For this aim, far-IR spectroscopy and DSC analysis of the dispersion of activation barriers to dynamics in the glass transition were applied, to our knowledge, for the first time for studying polymer nanolayers. These measurements were performed for interfacial PVP monomolecular layer with 1–2 nm thickness and for thicker shells, up to 10–20 nm.

2. Experimental section

2.1. Materials and preparing core–shell nanosamples

Fumed silica nanoparticles A-300 (99.87% purity, as obtained from the Pilot plant of the Institute of Surface Chemistry, Kalush, Ukraine, specific surface area $S_{BET} = 342$ m^2/g) were heated for 4 h at 450 °C to remove residual HCl and other adsorbed compounds. Commercial poly(vinyl pyrrolidone), PVP (Biopharma, Kiev, pharmaceutical purity, $M_n = 12{,}600 \pm 2700$ g mol^{-1}) was used as-received.

PVP/silica composites were prepared, as previously [53,54], in the pseudo-liquid state (PLS). A set of core–shell nanosamples with PVP content $C_{PVP} = 20$, 40, 80 or 90 wt% (labeled as 20PVP/80SiO$_2$, 40PVP/60SiO$_2$, 80PVP/20SiO$_2$, and 90PVP/10SiO$_2$, respectively) was obtained in the glass reactor fitted with a mixer (500–700 rpm). On addition of 50% aqueous solution of PVP to dry silica powder the gel-like systems were obtained which were stirred for 10 min, then placed into glass dishes, dried at 30 °C for 3 days and at 60 °C for 2 h, and dispersed in a microreducer for 10 min to obtain powder materials.

This procedure provides relatively uniform distribution of PVP on silica surface, i.e. a maximal amount of contacts between nanosilica surface and PVP molecules, in contrast to poor distribution of dry-state PVP. Basically low-density, highly-porous aggregates of individual silica core–PVP shell nanoparticles were formed at PVP content $C_{PVP} = 20$ or 40 wt%. In the case of $C_{PVP} = 80$ or 90 wt%, dense poreless nanocomposites with silica particles distributed in PVP matrix were obtained. The geometry of both these aggregates and the individual nanoparticles could be characterized using a few indirect methods.

2.2. Geometric/structural characterization

Low-temperature nitrogen adsorption (LTNA) analysis allowed to estimate the specific surface area, size distribution of individual silica nanoparticles, and the pore volume and size distribution in silica and PVP/silica nanoparticle aggregates. Additionally, the structural characteristics obtained from LTNA analysis were used to calculate the PVP shell thicknesses.

Low-temperature (77.4 K) nitrogen adsorption/desorption isotherms were measured using a Micromeritics ASAP 2405 N adsorption analyzer. The specific surface area of silica nanoparticles $S_{BET} = 342$ m^2/g was calculated by the standard BET method [51]. The pore volume V_p was estimated at $p/p_0 \approx 0.98$–0.99. Pore size distributions (PSD, $f_V(R)$ and $f_S(R)$ with respect to the pore volume and the specific surface area, respectively, where R is a pore radius) were calculated using the overall isotherm equation based on the Nguyen–Do equation for adsorbents with slit-like pores [55], modified for cylindrical pores and voids between spherical particles [56]. The $f_V(R)$ and $f_S(R)$ functions were used to calculate contributions of pores at $R < 1$ nm, at $1 < R < 25$ nm, and at $25 < R < 100$ nm to the specific surface area and the total porosity. The relevant calculations were described elsewhere [57–59].

Particle size distributions were studied by the quasi-elastic light scattering (QELS) method using a Zetasizer 3000 (Malvern Instruments) apparatus ($\lambda = 633$ nm, $\Theta = 90°$) and a ZetaPlus (Brookhaven Instruments) apparatus. Silica or PVP/silica powder water suspensions were prepared for this aim, as described in detail elsewhere [47]. As shown below, this technique allowed us to estimate the size of nanoparticle aggregates since the individual core–shell nanoparticles could not be observed.

Particle size polydispersity (PD) was calculated as PD $= \mu_2/\Gamma^2$, where $\mu_2 = (D^{2*} - D^{*2})q^4, \Gamma = Dq^2$, Γ is the decay rate, D^* is the average diffusion coefficient estimated as the first moment $\langle D\rangle = \sum Nm^2F(q,d)D/\sum Nm^2F(q,d)$ of the diffusion coefficient distribution, D^{2*} can be given as the second moment $\langle D^2\rangle = \sum Nm^2F(q,d)D^2/\sum Nm^2F(q,d)$, N is the number of particles, m is the particle mass, $F(q, d)$ is the particle form-factor dependent on the particle size d and the scalar of the wave scattering vector $q = 4\pi n/\lambda \sin\theta/2$, λ is the light wavelength, θ is the scattering angle (typically $\theta = 90$–$155°$), and n is the index of refraction of the suspending liquid.

PD values can be calculated on the basis of the QELS data in principle for any distribution of particles, e.g. primary particles, their secondary aggregates, as well as their mixtures. However, the core–shell particles studied easily formed particles as aggregates, and therefore PD characterized the sizes of particle aggregates.

To study the morphology of silica and PVP/silica particles, Atomic Force Microscopic (AFM) images were obtained using a NanoScope III (Digital Instruments, USA) apparatus with a tapping mode AFM measurement technique. Before AFM scanning, the dry powder samples were heated at 80 °C, cooled to room temperature and then

slightly smoothed by hand pressing using a glass plate. The latter procedure did not affect the structure of primary and secondary particles (aggregates or agglomerates) in the studied samples.

2.3. Differential scanning calorimetry (DSC)

Perkin–Elmer DSC-2 apparatus was used for the characterization of PVP glass transition in neat PVP and PVP/silica powders in the absence of water. Glass transition temperature T_g at the half-height of a heat capacity step, transition breadth $\Delta T_g = T_g'' - T_g'$, where T_g' and T_g'' are the temperatures of the glass transition onset and completion, respectively, as well as the heat capacity step ΔC_p, and the apparent activation energy Q dispersion for segmental motion within the glass transition were determined. The second scans were taken, in order to exclude the side endothermic effect of water desorption in a DSC curve and to deal with waterless samples. Typically, the heating rate $V = 20$ °C/min over the temperature range from 20 to 217 °C (scan I) or 250 °C (scan II) was used, and cooling was performed at the rate $V = 320$ °C. Additionally, some special thermal treatment regimes were used to investigate the physical aging effects. Activation energy Q values were determined, with the accuracy of 10%, by varying a heating rate V from 2.5 to 40 °C/min and using $\ln V$ versus T^{-1} (K^{-1}) linear dependencies, by the formula [33,60]:

$$Q = -R\frac{\mathrm{d}\ln V}{\mathrm{d}\left(T^{-1}\right)} \quad (1)$$

T_g, T_g'' or T_g' temperatures, that could most definitely be registered from the DSC curves, were chosen for the estimation of the activation energies.

2.4. Far- and mid-IR spectra

Previously [52–54], samples of silica and PVP/silica pressed with KBr into tablets were used for spectroscopic analysis in the mid-IR region (ThermoNicolet FT-IR spectrometer). To characterize interfacial interactions, the peculiarities of molecular dynamics and conformational state in PVP shells compared with those in bulk PVP, far-infrared spectra over the range from 20 to 500 cm^{-1} were registered in the present work using FIS-21 Hitachi spectrometer (resolution 1–2 cm^{-1}). Additionally, for registering the absorption bands, characterizing hydrogen bonding in the samples, the spectra in the region of 2600–3800 cm^{-1} were obtained using a Perkin–Elmer 577 spectrometer.

Low-density polyethylene (LDPE) matrix was used in these experiments as sufficiently transparent medium for far-IR spectroscopy, which besides isolated samples from atmospheric water. All samples were heated to 220 °C at the rate of 20 °C/min to remove water and then immediately cooled to room temperature with the rate of 320 °C/min. Then, the sample/LDPE powder mixtures (taken in the ratio of 1:100) were prepared, held for 3 h at 95–100 °C in the mould, and then heated up to 110 °C under slight pressure for melting LDPE and obtaining monolithic films. Unlike using waterless samples in the DSC experiments, in these experiments drying did not allow to remove water totally from silica surface and PVP, since some repeat water absorption by hydrophilic PVP inevitably occurred during the procedures on film preparing. As known, water is not a simple admixture in this system, and PVP/tightly-bound water complexes with H-bonding may be formed [61,62].

The following samples were prepared with LDPE matrix: neat silica; neat PVP; 40PVP/60SiO_2; 20PVP/80SiO_2 compositions as well as 20PVP/80SiO_2 composition annealed for 1 h at 150 °C (see below about a reason for the choice of this temperature). To obtain the spectra of neat PVP and PVP shells, the reference spectra of neat LDPE and LDPE/silica films, respectively, were obtained for the films with the same effective thicknesses of silica and PE as in the studied film samples. The film thicknesses varied (with taking the sample composition into account) in the range of about 100–300 μm for registering far-IR spectra, and of 10–30 μm at measurements of mid-IR spectra. Three repeat spectral measurements were performed in all cases.

The absorption coefficient k values were determined using the formula:

$$k = \frac{1}{d_{\mathrm{eff}}}\ln\frac{I_0}{I} \quad (2)$$

Here d_{eff} is the effective thickness of PVP layer estimated from the sample composition; I is the transmission of a studied film, and I_0 is the transmission of a reference film (LDPE or LDPE/silica).

3. Results and discussion

3.1. Samples' characteristics

Fig. 1 shows that the size of primary silica particles had relatively narrow distribution varying from 6 to 16 nm. The primary silica and PVP/SiO_2 nanoparticles formed secondary structures, basically as porous aggregates, due to hydrogen bonding and electrostatic interactions between uncovered silica nanoparticles and sticking of PVP/SiO_2 particles after their treatment in the pseudo-liquid state. Fig. 2 shows the AFM images of silica and 20PVP/80SiO_2 samples manifesting relatively uniform aggregates of primary particles of ~50–100 nm in size; the individual nanoparticles of 6–16 nm size could not be discerned. Fig. 3 shows typical size distribution of 20PVP/80SiO_2 nanoparticle aggregates in water dispersion obtained from the QELS measurements; PVP shell was irreversibly adsorbed by silica surface in this case. Two-modal particle size distribution is observed, with the aggregates of ~100 nm and 500–800 nm in size.

It was found that the bulk density of the initial powder of fumed silica equaled 0.03–0.06 g/cm^3 only. It increased to 0.1–0.3 g/cm^3

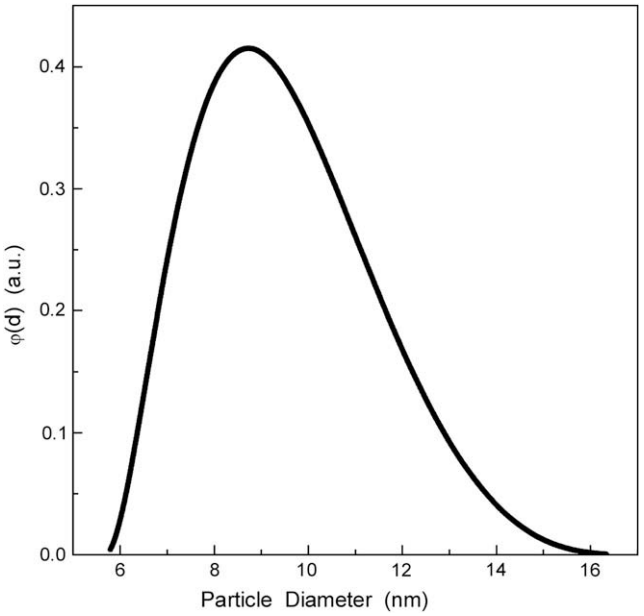

Fig. 1. Size distribution of individual silica nanoparticles as estimated by LTNA.

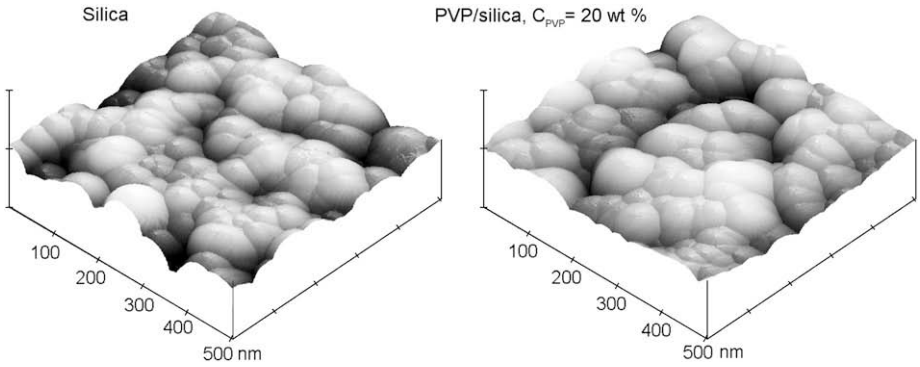

Fig. 2. Typical AFM images (500 × 500 nm) of the aggregates of silica (on the left) and 20PVP/80SiO_2 nanoparticles (on the right). The latter were obtained by the treatment of PVP/silica mixture in the pseudo-liquid state.

for PVP–silica aggregates with 20 or 40 wt% PVP, but with increasing PVP content more conjugated structures were formed. At 80–90 wt% PVP, the samples had almost "normal" high density since practically non-porous microparticles of nanocomposites were obtained.

LTNA isotherms also showed that the specific surface area $S_{BET} = 342$ m^2/g for initial silica aggregates decreased by 30–40% for the 20PVP/80SiO_2 samples and by 75% for the 40PVP/60SiO_2 samples. At 80 or 90 wt% PVP, specific surface area of samples dropped down to about 1 m^2/g. The schemes of the nanostructures of the PVP/silica samples with 20 and 90 wt% PVP are given in Fig. 4.

The morphologies of silica and 20PVP/80SiO_2 particles were very close since their LTNA isotherms were of the same type. Fig. 5 shows the typical pore size distributions (PSDs) for the nanoparticle aggregates calculated on the basis of the experimental LTNA isotherms. In both cases, the radius of "pores" (voids, slits) between primary particles in secondary ones varies from 0.3 to 100 nm. However, PSD function of the PVP-covered silica differs from that of the initial silica powder. Thus, the volume of pores with pore radius $R_p < 1$ nm slightly decreased, due to the penetration of PVP molecules into the silica aggregates, inside gaps between the adjacent primary nanoparticles. Presence of PVP results also in some redistribution between the main PSD peak at 10 nm and the volume of pores with R_p of a few nanometers. The largest impact of the PVP presence is a substantial increase in the volume of larger pores with $R_p > 20$ nm, due to the changes in the packing of nanoparticle aggregates.

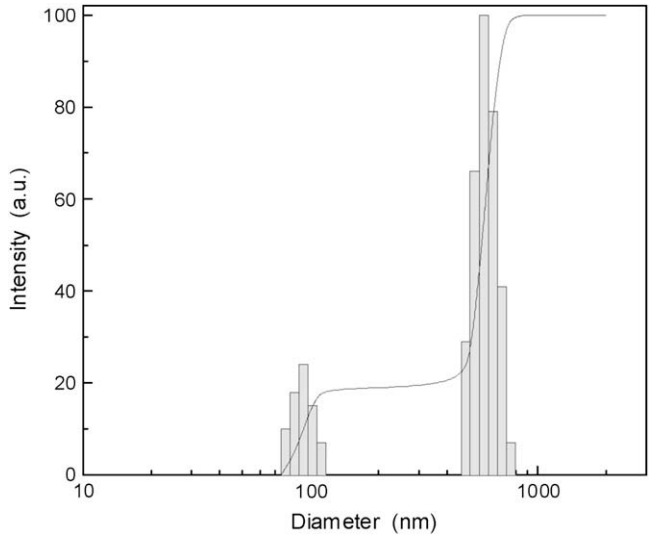

Fig. 3. 20PVP/80SiO_2 nanoparticle aggregates: typical size distribution with respect to light scattering (QELS measurements) as measured in the 0.5 wt% aqueous suspension.

At last, the structural data, obtained from the combined LTNA/AFM/QELS/density analysis, were used for the calculation of the PVP shell thicknesses as a function of PVP content in the samples. Shell thicknesses were calculated for two boundary cases: (i) individual non-aggregated primary silica nanoparticles covered by PVP, and (ii) PVP-covered aggregates of silica nanoparticles. The real thickness of the PVP layer must be between these two boundary cases. For samples with 20 or 40 wt% PVP, the shell thickness is more close to the lower values (boundary 1) since PVP molecules can easily penetrate into the inner space of aggregates, and a major portion of silica is present as aggregated PVP-covered nanoparticles with relatively uniform polymer shells. At the same time, at $C_{PVP} = 80$ or 90 wt% PVP the thickness of a polymer layer between individual silica nanoparticles must be increased by a factor of 2, as a consequence of compacting PVP-covered silica particles.

Fig. 6 shows the dependence of PVP shell thickness, h_{PVP}, on a polymer fraction in the nanocomposites studied. It is represented with the shaded area, and $h_{PVP} = 1$–2, 2–5, 5–15, and 8–25 nm at $C_{PVP} = 20$, 40, 80, and 90 wt% PVP, respectively, for the models with PVP coverage of non-aggregated, individual spherical primary particles (the lower boundary h_{PVP} value) and for the covered aggregates (the upper boundary h_{PVP} value). It is noteworthy that the radius of gyration of PVP macromolecule $R_g = Ll/6 \approx 8$ nm, where $l \sim 2$ nm is the Kuhn segment length, and contour chain length $L = 25$ nm for used PVP with $M_n = 12{,}600$ g mol^{-1}. Therefore, the most interesting composite with $C_{PVP} = 20$ wt% PVP was characterized, obviously, with the presence of practically monomolecular shell layer with a flattened conformation [52–54].

Of course, shell uniformity problem remains, to some extent; however, the FT-IR measurements and other data presented below assume rather uniform distribution of PVP molecules on silica surface at preparing these core–shell particles in the PLS process.

3.2. PVP–silica interactions as estimated from mid- and far-IR spectra

The physical interfacial interactions in the core–shell particles under study are controlled, besides the contribution of London dispersion forces, by strong hydrogen (H–) bonding between PVP and silica surface, and also, presumably, by "soft" Lewis acid–base attractive forces, as is discussed below.

Previously [52–54], FT-IR spectroscopy has been used to study in detail H-bonding between pyrrolidone rings of PVP and silanols of silica surface (NC═O···HOSi) in different routes of the formation of PVP–silica nanoparticles, including mechanical mixing of relatively

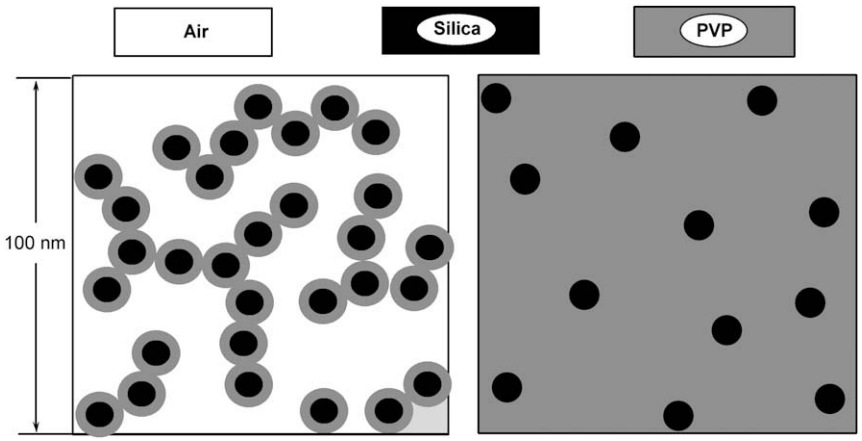

Fig. 4. A scheme of the nanostructures of PVP/silica samples studied with 20 wt% PVP (on the left, density of ~0.1 g cm^{-3}) and with 90 wt% PVP (on the right, high-density nancomposite).

dry polymer and silica powders and the PLS treatments of these mixtures. The H-bonding degree was controlled from the changes in a narrow IR band $\nu_{O-H} = 3730–3750$ cm^{-1} of silanols free from hydrogen bonds.

The FT-IR spectra of dried silica powder/PVP mixtures were akin to that of the neat silica that evidenced the absence of PVP distribution on the silica surface (or poorly distributed PVP) and weak interaction between them [52]. The spectrum of such "dry" 20PVP/80SiO$_2$ sample in the 2800–3800 cm^{-1} range includes, besides a few overlapping O–H stretching vibration bands corresponding to silanols disturbed by H-bonds, also the intense narrow band of free silanols at 3730–3750 cm^{-1} (Fig. 7a).

After PLS treatment (prolong exposition of 20PVP/80SiO$_2$ mixture in the saturated vapors of ethanol, water or their mixture), the picture of PVP distribution on silica surface cardinally changed. Swelling of PVP led to an increase in the segmental mobility and to migration of molecules with their redistribution between silica surface places previously covered by PVP and free of PVP. This time-dependent rearrangement of the adsorbed PVP molecules caused the formation of a relatively uniform and dense adsorption layer (polymer nanoshell) at the silica surface. Of importance, PVP monomolecular layer coverage of silica nanoparticles just corresponds approximately to $C_{pvp} = 20$ wt% in the core–shell nanoparticles, and PVP molecules could not be washed off practically from the silica surface in this case (the irreversible adsorption).

As a result, practically all silanols on silica surface are disturbed already on the adsorption of 20 wt% PVP, due to the interaction with PVP and, besides, partly with residual tightly-bound water. This PVP redistribution process and PVP–silica hydrogen bonding were confirmed by decreasing and total disappearance of the absorption band at 3730–3750 cm^{-1} in the spectrum of uniform PVP shell (Fig. 7a); simultaneously, increasing a broad band with maximum at 3340–3400 cm^{-1} of silanols, participating in the H-bonding, is observed. Of course, disappearance of the band at 3730–3750 cm^{-1} was observed also for the thicker PVP shells.

Additionally, Fig. 7b shows the absorption band ν_{O-H} of free silanols in the spectra of dried powder samples sealed into LDPE in this work (the core–shell samples were treated in pseudo-liquid

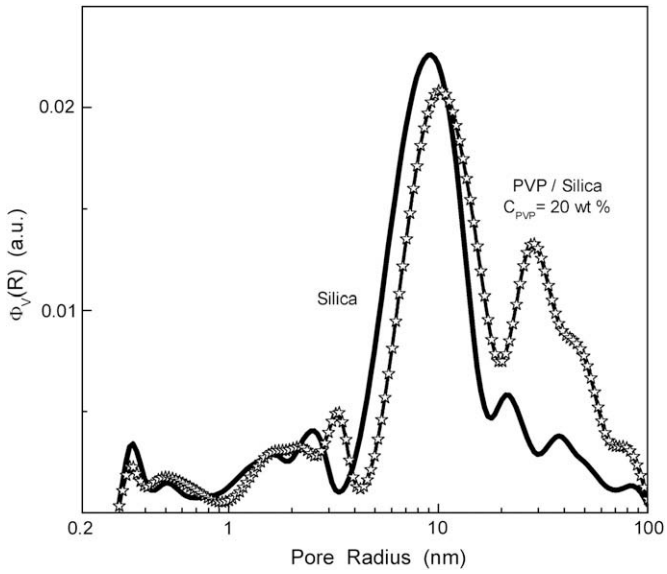

Fig. 5. Typical "pore" size distributions in the aggregates of silica and 20PVP/80SiO$_2$ nanoparticles obtained in the pseudo-liquid state.

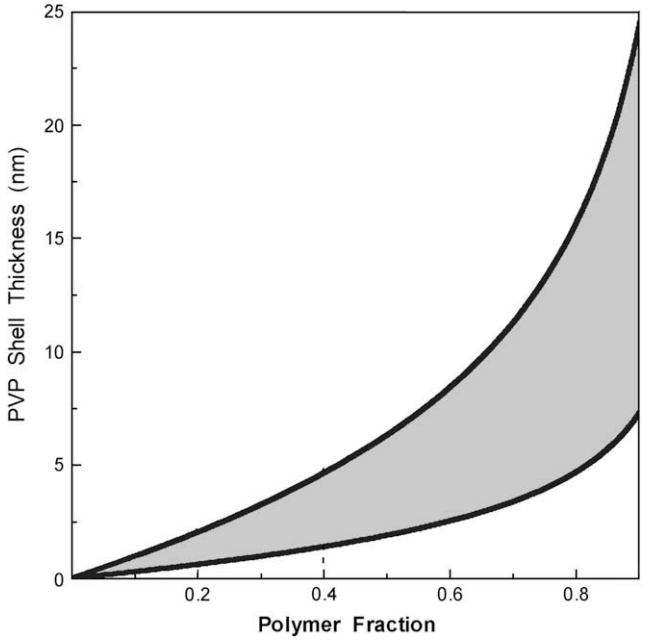

Fig. 6. PVP shell thickness as a function of polymer fraction in PVP/SiO$_2$ particles. Lower values of the shaded area relate to uniform PVP coating of individual non-aggregated silica nanoparticles, and the upper ones relate to PVP shells in the particle aggregates. The thicknesses were calculated from the LTNA analysis data.

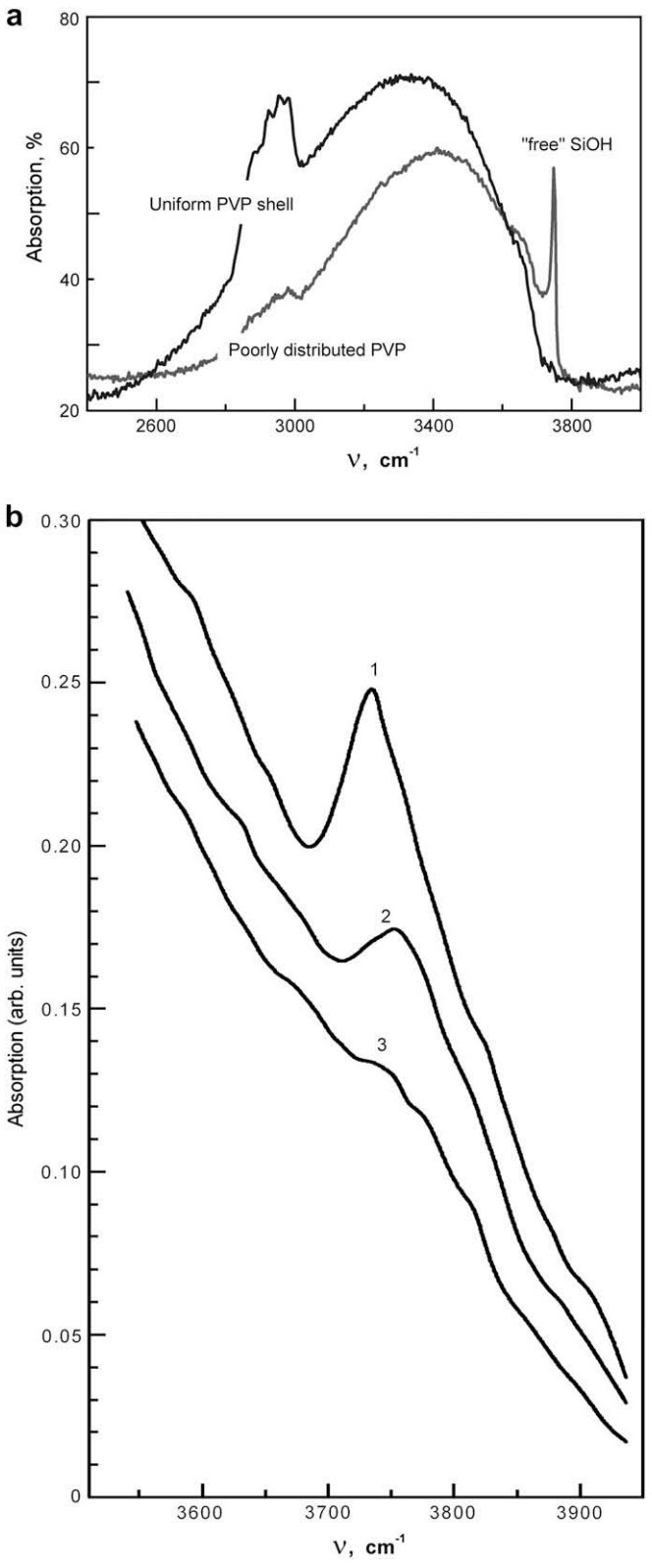

Fig. 7. Mid-IR spectra of uncovered silica and 20PVP/80SiO_2 particles in the region of the absorption bands of SiOH groups: (a) FT-IR spectra of the 20PVP/80SiO_2 samples (pressing in KBr tablets) before (1) and after (2) exposition powders in saturated vapour of water/ethanol mixture (1:1) (pseudo-liquid state), that is, with poor and uniform distribution of PVP at silica surface, respectively [52]; (b) the absorption band $\nu_{(O-H)}$ of free silanols in the spectra of powder samples prepared as indicated in Section 2.1 and sealed into LDPE: (1) uncovered silica nanoparticles; (2) 20PVP/80SiO_2 sample, and (3) 20PVP/80SiO_2 sample annealed for 1 h at 150 °C before mixing with LDPE. All sample/LDPE mixtures were dried, additionally, for 3 h at 100 °C directly before sealing (melting LDPE).

state as indicated in Section 2.1). This absorption band is observed distinctly for uncovered silica nanoparticles; it strongly decreases for the 20PVP/80SiO_2 sample and practically disappears if the sample was annealed for 1 h at 150 °C before mixing with LDPE.

According to quantum chemical calculations, the interaction energy between PVP molecules equals 7 kJ/mol [54], whereas H-bond enthalpy in PVP–H_2O complexes equals 25 kJ/mol [61], and the energy of hydrogen bonds between NC═O groups of PVP and SiOH groups of silica surface ranges from ca. 40 to 50 kJ/mol [54]. Such different interactions explain the effects of (a) the facilitated formation of PVP–water complexes, and (b) the preferable adsorption of PVP molecules (in the pseudo-liquid state) onto uncovered silica surface. The multi-fold difference in the PVP–PVP and PVP–silica interaction energies may be considered as the main driving force of the process of PVP redistribution onto silica surface and the formation of uniform PVP nanoshell.

New information on the interfacial interactions and dynamics at interfaces was obtained from the far-IR spectra of PVP and PVP shells with 1–2 and 2–5 nm thicknesses, i.e. in the 20PVP/80SiO_2 and 40PVP/60SiO_2 samples. To our knowledge, far-IR spectra of both PVP and of adsorbed monomolecular polymer layers at all were registered in this work for the first time. The spectra obtained and the results of their analysis are presented in Fig. 8 and in Tables 1 and 2.

Seven partly overlapping absorption bands with the maxima at 42, 83, 100, 170, 247, 355 and 446 cm^{-1} can be seen in the far-IR spectrum of neat PVP. Their assignments could be done (Table 1) with the certainty, or tentatively to some extent, in the following ways.

The doublet adsorption band 83 and 100 cm^{-1} relates to the hindered, small-angle torsional vibrations (librations or Poly-type absorption) of a repeat monomer unit of PVP chain, with the basic contribution of pyrrolidone ring to this motion. Really, for linear polymers with carbon–carbon backbone chains and ring and/or polar side groups (PS, PMS, PMMA, PMA, PVAc and others) the frequencies of librations ν_{libr} were registered just in the ca. 80–100 cm^{-1} range [63,64]. Besides, the validity of this assignment we confirmed by the calculations. As shown [64], librational motion frequency may be determined, using a simple Brot–Darmon model, from the formula:

$$\nu_{libr} = (nc\varphi)^{-1}(Q/2I)^{1/2} \quad (3)$$

where φ is a librational angle, Q is a potential barrier of libration, I is a moment of inertia of monomeric unit, and c is the light velocity. The ν_{libr} value for PVP was estimated from the relations for $Q = E_{coh}/3$ [64], $I = 2mR^2/5$, and $\varphi = 12.5°$ (libration angle is typically equal to 10–15°). Here $E_{coh} = 26$ kJ/mol is PVP cohesion energy, and m and R are the molecular weight and the equivalent radius of PVP monomer unit, respectively. The calculation showed that the expected value of ν_{libr} equaled around 80 cm^{-1}, indeed.

The doublet structure of librational absorption band in the neat PVP spectrum may be explained by the complicated conformational state of macromolecules. Similar splitting of librational band with the difference in the ν_{libr} values of 10–20 cm^{-1} has earlier been observed and explained with the existence of two isomeric states [64–66].

Far-IR spectra allow a direct analysis of low-frequency vibrations of the hydrogen bonds: the H-bond stretching and torsional vibrations are manifested typically at 110–180 and 40–60 cm^{-1}, respectively; the H-bond stretching vibrations at 190–250 cm^{-1} were registered only for carboxylic acids [64]. Therefore, the absorption bands 169 and 42 cm^{-1} in the neat PVP spectrum may be assigned to the vibrations of strong H-bonds in PVP complexes with tightly-bound residual water molecules.

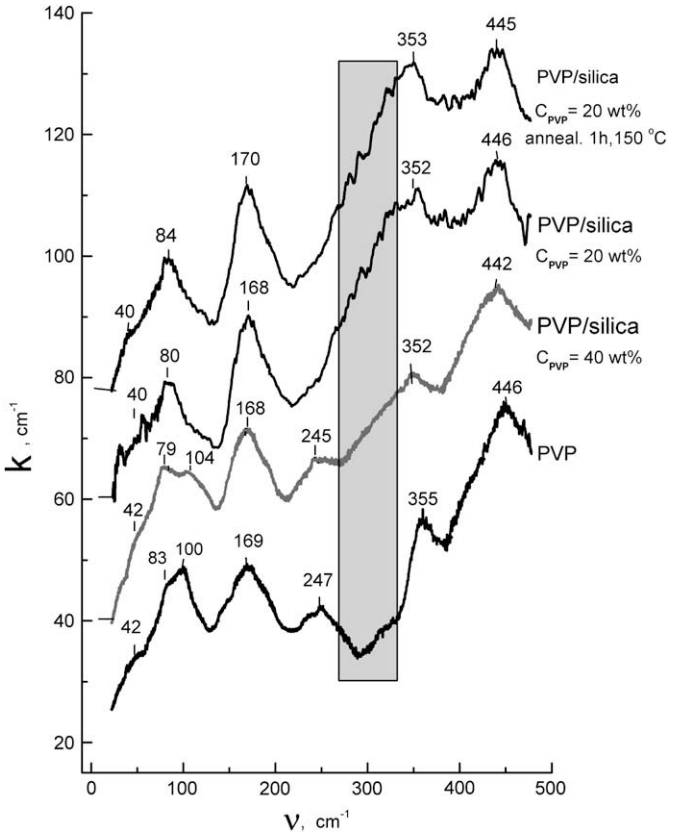

Fig. 8. Far-infrared spectra of neat PVP (1) and PVP shells in the PVP/silica samples with $C_{PVP} = 40$ wt% (2), 20 wt% (3), and 20 wt%, after annealing for 1 h at 150 °C before sealing into LDPE (4). Spectra 2, 3 and 4 are shifted relative to spectrum 1 along the ordinate axis.

Further, for linear polymers with carbon–carbon backbone chains and ring and/or polar side groups torsional skeletal vibrations determine the absorption bands over the 200–250 cm^{-1} range [64]; therefore, the band at 247 cm^{-1} in the spectrum of neat PVP may be associated with these vibrations. The absorption bands at 355 and 446 cm^{-1} may be assigned, with a large probability, to deformation vibrations of pyrrolidone rings. Finally, the spectral changes within the ~250–350 cm^{-1} range, associated probably with Lewis acid–base interactions, are considered below.

Fig. 8 and Tables 1 and 2 demonstrate the changes in the PVP far-IR spectrum when PVP was transformed into nano-dispersive state, i.e. for 1–2 and 2–5 nm thick PVP shells adsorbed at silica surface.

Table 2
Far-IR characterization of PVP–silica interfacial interactions.

Sample	H-bonds	PVP/silica Lewis acid–base interactions (~250 to 350 cm^{-1} region)		
	k_{170}/k_{80}	k_{318}/k_{80}	k_{350}/k_{80}	k_{350}/k_{444}
PVP	1.06	0.85	1.15	1.15
40PVP/60SiO_2	1.14	1.20	1.23	0.82
20PVP/80SiO_2	1.22	1.50	1.31	0.92
20PVP/80SiO_2 (annealed at 150 °C)	1.25	1.53	1.35	0.96

Note. The k_{80} and k_{444} values and their ratio remained practically constant.

Table 1 presents the frequencies in the band maxima, whereas the ratios of the absorption coefficients are given in Table 2.

One can see the significant changes in the spectra relating to dynamics and conformational state of chains at the interfaces, and to interfacial interactions. Moreover, these changes basically increase in a row: neat PVP – 2–5 nm thick shell (40PVP/60SiO_2 composition) – 1–2 nm thick monomolecular shell (20PVP/80SiO_2 composition) – 20PVP/80SiO_2 sample annealed for 1 h at 150 °C. Two points must be noted herein. The absorption coefficients k of the bands with the maxima at 442–446 cm^{-1} and around 80 cm^{-1} remained practically unchangeable, and therefore we calculated the ratios of the other absorption band coefficients to these ones. And, secondly, the temperature 150 °C was chosen for annealing PVP monolayer shell, because dried PVP, containing only residual tightly-bound water, may change the conformation, with the extension of backbone chain, just at this temperature [61]. We supposed that it may promote formation "trains" and enhance PVP–silica interfacial interactions.

As a matter of fact, four results may be extracted from the far-IR spectra presented.

First, for monomolecular PVP shell with 1–2 nm thickness (at 20 wt% PVP) the doublet absorption band of librational motion transforms into the single band at ~80 cm^{-1} and, besides, some suppression of torsional skeletal vibrations is observed since the absorption band 245–247 cm^{-1} disappears. We suppose that these changes are associated with "simplifying" conformational state of the majority of PVP segments in adsorbed monolayer (flattened conformations and extended chains), and with prevailing "trains" strongly interacting with silica surface.

Far-IR spectra distinctly confirm, indeed, increasing the number of H-bonds between NC=O groups of pyrrolidone rings and silanols of silica surface (Fig. 8 and Table 2). The intensity of the absorption band of H-bonds at 168–170 cm^{-1} increases in the same row: neat PVP – 2–5 nm shell (40PVP/60SiO_2 composition) – 1–

Table 1
Absorption bands (cm^{-1}) in far-IR spectra of PVP in bulky state and nanoshells.

Sample	Small-angle librations	H-bonds[a]		Torsional skeletal vibrations	PVP/silica Lewis acid–base interactions[b]	Deformation vibrations of rings	
		Stretching vibrations	Torsional vibrations				
PVP particles	83, 100	170	42	247	–	355	446
PVP nanolayer (h_{PVP} = 2–5 nm)	79, 104	168	42	245	~250 to 350	352	442
PVP nanolayer (h_{PVP} = 1–2 nm)	80	168	40	–	~250 to 350	352	446
PVP nanolayer (h_{PVP} = 1–2 nm) Anneal. 1 h, 150 °C	84	169	40	–	~250 to 350	353	445

[a] H-bonds in neat PVP must be assigned to PVP-residual water complexes.
[b] Tentative assignment (see discussion in text).

2 nm monomolecular shell (20PVP/80SiO_2 composition) – 20PVP/80SiO_2 annealed for 1 h at 150 °C. The k_{170}/k_{80} ratio increases from 1.06 to 1.25. Most tight attaching PVP segments to silica surface, via H-bonds (cooperative H-bound interaction), may be presumed after annealing PVP monolayer at 150 °C. Such supposition turned out to be in accordance with the DSC analysis of dynamics (see next section).

And last but not least effect, observed in the far-IR spectra of PVP nanoshells, is arising of the pronounced additional absorption in the broad spectral range between ca. 250 and 350 cm^{-1}. Its intensity increased, again, in the same row of samples that may be seen distinctly from the ratios of the absorption coefficients, k_{318}/k_{80}, k_{350}/k_{80}, and k_{350}/k_{444} (Fig. 8, Table 2); here, k values at 318 and 350 cm^{-1} were taken arbitrarily as reference points within the 250–350 cm^{-1} spectral range. We suppose this effect may tentatively be assigned to the manifestation of "soft" Lewis acid–base interactions between silica surface and adsorbed PVP segments (trains) strongly attached to silica substrate.

As known, the current approaches to adsorption, adhesion and mixing polymers with the other materials (fillers, pigments, etc.) are based to a large extent on the ideas of Lewis acid–base interactions [67–69]. In particular, such interactions at the interfaces between oxides and polar polymers are discussed [70–72], including carbonyl-containing polymers on silica substrates, e.g. PMMA [70,71] and PVP [72]. Interestingly, the development of such acid–base adducts can induce extending chains and simplifying conformation set, e.g. backbone *trans–gauche* conformation changed into *trans–trans* conformations for PMMA [70]. Of importance, PVP is considered as a rather strong Lewis base [73].

On the other hand, fumed silica nanoparticles, obtained under ultrahigh-temperature conditions, may contain, along with the single silanol groups (manifesting slight acidity), also rare twin silanols (manifesting the enhanced acidity) and the active sites on surface silicon atoms as electron deficient Lewis acid centers [74]. It was shown that adsorption of different polar organic probes on a partly dehydroxylated silica surface occurred through Lewis interactions [75].

And the last argument in favor of our assignment of new absorption at ~250–350 cm^{-1} to Lewis interactions at PVP/silica interface is as follows. The stronger Lewis interfacial interactions may be expected for the adsorption of PVP at metal oxide substrates [76]. The investigations of PVP adsorption onto alumina, titania, or iron oxide showed that the adsorption mechanism in these cases is controlled basically with the Lewis acid–base interactions between a substrate surface and NC═O groups of PVP as a Lewis base [72]. From this viewpoint, our recent far-IR experiments, performed for 20PVP/80Al_2O_3 nanoparticles, are of interest. It was revealed that the absorption at ~250–350 cm^{-1} was, really, more pronounced in this case than for PVP/silica nanoparticles [77], in accordance with the above assignment of this absorption.

Thus, it may be assumed that two basic modes of interfacial forces may be considered (besides London dispersive forces) at PVP adsorption on silica: (i) single or cooperative H-bonds of pyrrolidone rings with silica surface hydroxyls, and (ii) adsorption with electron transfer at Lewis acidic sites. Very strong PVP/silica interfacial interactions and peculiar conformational state of adsorbed polymer at the level of monomolecular layer may crucially affect the manifestation of segmental dynamics at interfaces. This is confirmed, indeed, by the DSC experiments presented below.

3.3. DSC: glass transition dynamics in PVP nanoshells

Fig. 9 shows DSC curves obtained at cooling of neat PVP and 20PVP/80SiO_2 nanoparticles in the temperature range covering the glass transition region. Their cardinal difference is obvious: at cooling the 20PVP/80SiO_2 sample the end of strongly extended transition range could not be registered, evidently, because of the difficulty of revealing distinctly this temperature point in this case. That already assumes the peculiar glass transition dynamics in the PVP/silica samples.

Really, Fig. 10 demonstrates large differences in the DSC curves obtained at heating for waterless PVP and core–shell samples studied. Generally, a strongly broadened, up to $\Delta T_g = T_g'' - T_g' = 108$ °C, and two-stage glass transition are observed for PVP shells unlike $\Delta T_g = 18$ °C for neat PVP. Glass transition extends in both directions, to lower temperatures, down to temperatures of 63–76 °C, approximately corresponding to the temperatures of β - relaxation in PVP, and by about 20 °C to higher temperatures. Lower-temperature stage 1 of accelerated dynamics and the higher-temperature stage 2 of slowed down dynamics, being observed in three cases for the PVP shell glass transition, are conditionally separated with the vertical dashed line in Fig. 10. The narrow glass transition in neat PVP may be conditionally related, by its temperature location, to stage 2. The strongly broadened but one-stage transition is observed for monomolecular PVP shell (at 20 wt% PVP in the core–shell particles). It should be stressed that the simple dependence of T_g on shell thickness is not observed in this case. It should also be noted that the anomalous glass transition was not associated with nanoparticle aggregation but only with the presence of PVP nanolayer at silica surface: the largest effect is observed at 20 wt% PVP when the particle aggregation is minimal (Fig. 4), and the enormous specific surface area remains.

Fig. 11 shows the dependencies of heat capacity step ΔC_p in the PVP glass transition on silica content in PVP/silica particles. Here the ΔC_p values were calculated for PVP mass fraction only and separately for stages 1 and 2. One can see that the relative contribution of the stage 1 of accelerated dynamics to the total ΔC_p step increased for the 20PVP/80SiO_2 sample but the total ΔC_p step remained unchangeable for all compositions.

Recently, it was revealed for some nanocomposites that physical aging rate can be dramatically reduced at interfaces relative to that in neat polymers, if strong polymer–substrate interactions are present [15,78]. A series of the DSC curves presented in Fig. 12 reveal, indeed, a special behavior of PVP shells (especially, monomolecular layer) regarding the physical aging.

Fig. 12a shows that the thermal treatment of neat PVP for different times at temperature a bit lower glass transition range (at

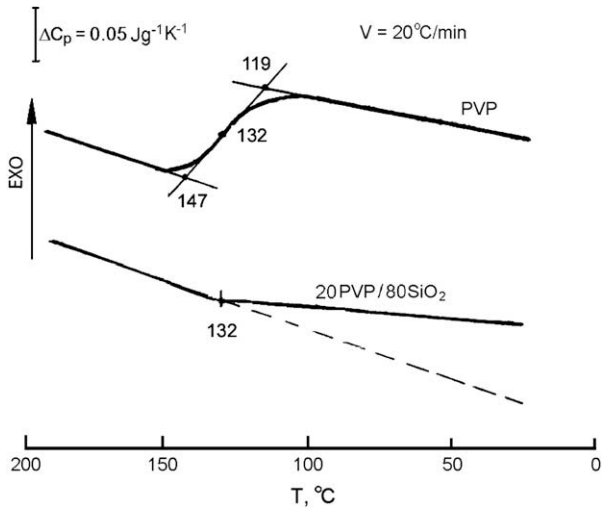

Fig. 9. DSC curves obtained at cooling of neat PVP and 20PVP/80SiO_2 nanoparticles at temperatures from 200 to 20 °C with the rate $V = 20$ °C/min.

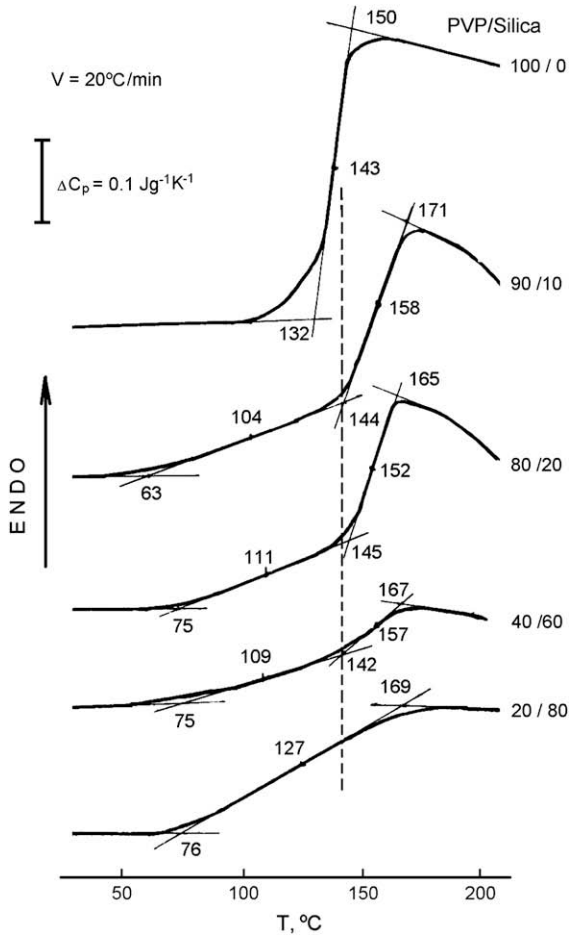

Fig. 10. DSC curves obtained at heating with the rate $V = 20$ °C/min for neat PVP and four compositions of PVP/SiO_2 nanoparticles. The second scans were taken after heating samples to 217 °C with the rate $V = 20$ °C/min and subsequent cooling down to 20 °C with the rate $V = 320$ °C/min. Two-stage heat capacity steps are observed for core–shell samples. Stages 1 and 2 are conditionally separated with the vertical dashed line.

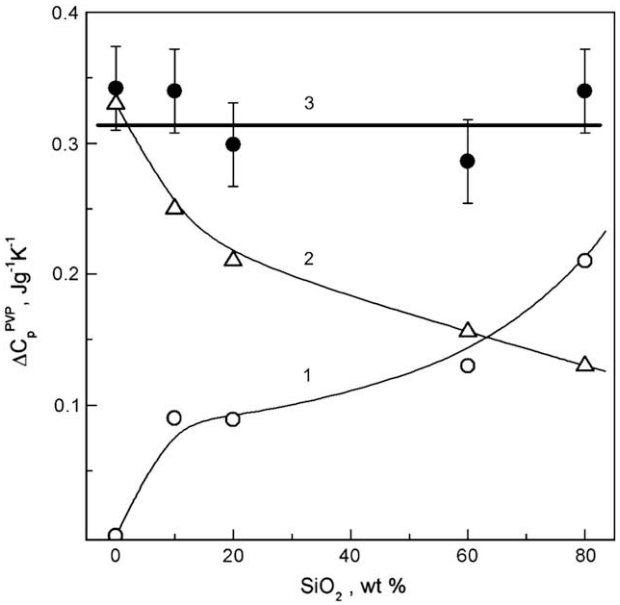

Fig. 11. Heat capacity step in the PVP glass transition of neat PVP and PVP/SiO_2 particles as a function of silica content (calculated for PVP mass fraction from the data presented in Fig. 10). (1) Lower-temperature step. (2) Higher-temperature step. (3) Total heat capacity step.

125 °C) led to manifesting the "normal" process of enthalpy relaxation, that is, arising and a gradual increasing the endothermic peak with T_{max} close to T_g'' (curves 1–4). Some changes in the aging process may be seen after the thermal treatment at different temperatures (100, 125 and 150 °C) of PVP/silica particles with 90 or 40 wt% PVP; nevertheless, aging occurred more or less in an usual way in these cases as well.

Meanwhile, for the monomolecular shell (20 wt% PVP) the different behavior of the glass transition after annealing was revealed. The treatment for 1 or 3 h at 125 °C did not change its DSC curve at all indicating suppression of aging process (Fig. 12a, curve 9). After the treatment at 150 °C, the endothermic peaks did not arise in the DSC curve as well; however, the time-dependent arising of a new heat capacity step at about 200–230 °C was distinctly observed (Fig. 12b), that is, two-step transition was formed. The magnitude of this new, high-temperature ΔC_p step corresponded approximately to one-second of the basic step located in the range of 81°–177 °C. Repeat scanning of this treated sample, after its heating to 250 °C and cooling with the rate of 320 °C, resulted, however, in disappearance of this new ΔC_p step. In this case a single ΔC_p step started then from 77 °C and ended only at 197 °C (instead of 169 °C for the initial samples, compare curves 1 and 5 in Fig. 12b).

The strongly broadened, complicated glass transition in waterless PVP shells, covering in particular the temperature range ΔT_g up to ~150 °C for thermally treated 1–2 nm thick PVP shell, is of large interest. It might be assumed that such transition width was associated with the contributions of a few different dynamic modes to the process of unfreezing mobility within the glass transition. These modes may, obviously, correspond to "normal", accelerated and slowed down dynamics. Such expectations are natural since PVP nanoshells may include "trains" more or less strongly attached, via H-bonds and Lewis interactions, to silica surface, as well as molecular loops and tails. Additionally, different molecular packings (local densities) are possible in these nanocomposites, and two types of interfaces, polymer–silica and polymer–air, are present in such systems.

These suppositions were corroborated in the DSC experiments performed at different heating rates and aimed at the determination of the values of apparent activation energy Q for segmental dynamics and their dispersions within the glass transition range. As indicated above, Q magnitudes were determined by the displacement of T_g, T_g'' or T_g' with a heating rate. These temperatures were chosen so that they could definitely be registered from the DSC curves.

Fig. 13 presents a large series of the PVP glass transition temperature versus ln V plots measured for waterless neat PVP, 20PVP/80SiO_2, 40PVP/6080SiO_2, and 80PVP/20SiO_2 compositions. The surprizingly different slopes of these linear dependencies suggest the changeable apparent activation energy Q for these compositions and, thereto, imply the heterogeneity of segmental dynamics within the broadened glass transition of a shell in an each of the PVP/silica compositions. The Q values were calculated using these data and formula (1).

Fig. 14 presents the obtained dispersions of apparent activation energies for segmental motion within the PVP glass transition, over the temperature range from about 70°to 230 °C. The dashed line corresponds to Arrhenius relation (activation entropy $\Delta S = 0$) between Q and temperature for non-cooperative relaxations under the conditions of DSC experiments, that is, for the equivalent frequency of about 10^{-2} Hz. The departure of Q from the $\Delta S = 0$ prediction line characterizes, other things being equal, the degree of intermolecular motional cooperativity in the glass transition region.

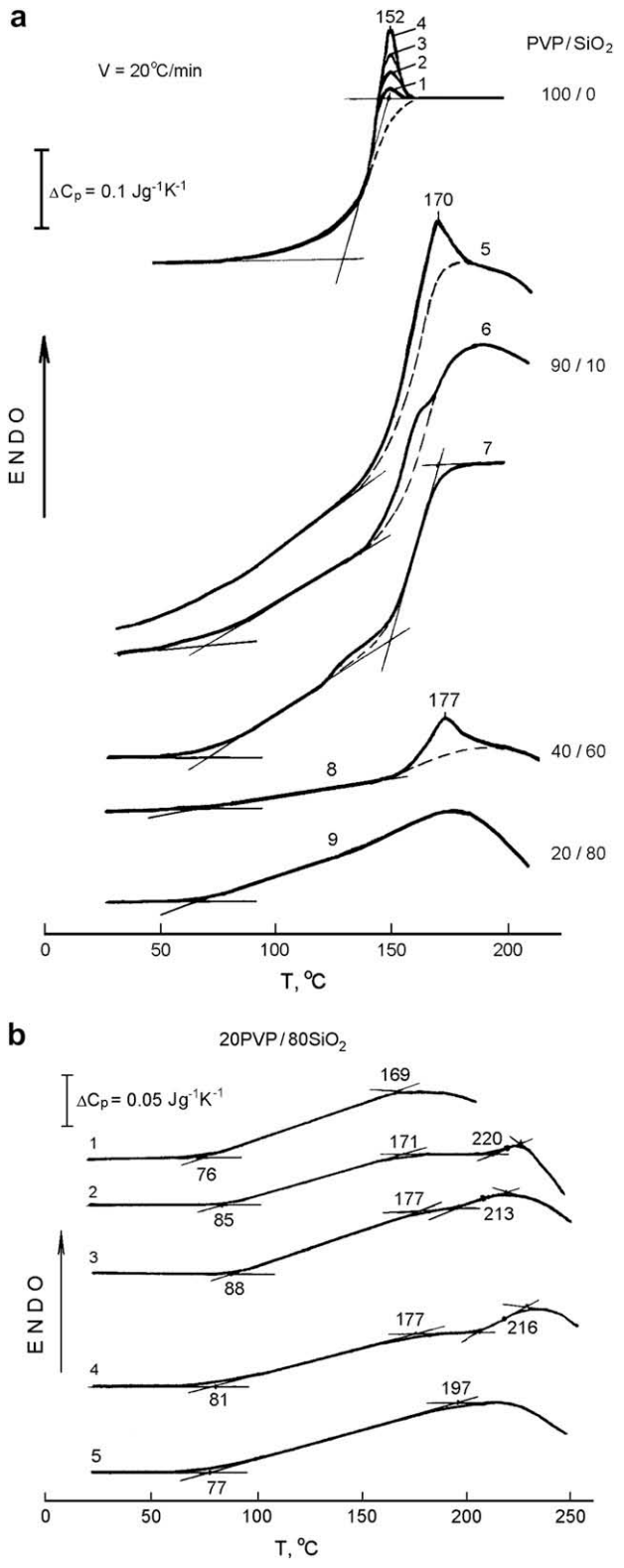

Fig. 12. Physical ageing in neat PVP and PVP/SiO_2 samples, as illustrated by enthalpy changes in the DSC curves (endothermic peaks' area): a: after thermal treatment for 5, 15, 30 min and 1 h at 125 °C (1–4); for 1 h at 150 °C (5), 125 °C (6), or 100 °C (7); for 1 h at 150 °C (8), and for 1 or 3 h at 125 °C (9, no effect). Dashed line corresponds to the subsequent scanning. b: before (1) and after treatment for 10 min (2), 23 min (3), or 1 h at 150 °C (4). Curve 5 is repeated scanning of treated sample after cooling from 250 to 20 °C.

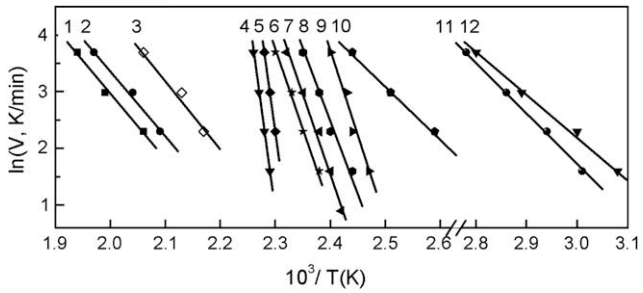

Fig. 13. PVP glass transition temperatures versus ln *V* dependencies obtained for: 1, 2, 3 – T_g'', T_g and T_g' in the new high-temperature transition in 20PVP/80SiO_2. 4, 5 – T_g'' in 20PVP/80SiO_2 and 40PVP/60SiO_2, respectively. 6 – T_g in neat PVP. 7, 8, 9 – T_g'', T_g and T_g', respectively, in the steep heat capacity step 2 for 80PVP/20SiO_2. 10 – T_g for 20PVP/80SiO_2. 11, 12 – T_g' for 20PVP/80SiO_2 and 40PVP/60SiO_2, respectively.

Fig. 14 shows a "normal" dynamic behavior for neat PVP where one-mode dynamics within a relatively narrow glass transition (~130–150 °C) is observed: the energy $Q = 250$ kJ/mol, as determined for the onset, middle or end of the transition range, typical of cooperative dynamics. In contrast, glass transition dynamics in PVP shells dramatically altered: the pronounced dynamic heterogeneity is revealed as it follows from the extremely wide *Q* dispersions in the broadened transition ranges. In turn, this suggests a very wide distribution of segmental relaxation times.

Fig. 14 shows that the $Q(T)$ dependencies strongly differ for the shells with different thicknesses. Generally, glass transition dynamics in the shells may be considered as at least two- or three-modal one. So, for the non-porous nanocomposite with 80 wt% PVP two relaxation modes are detected, "normal" (as for neat PVP, $Q = 250$ kJ/mol) and ultra-fast, non-cooperative Arrhenius one at 75 °C with. $Q = 75$ kJ/mol. On the contrary, normal cooperative dynamic mode, peculiar to bulk PVP, is absent in the glass transitions of the nano-porous 40PVP/60SiO_2 and 20PVP/80SiO_2 samples with 2–5 and 1–2 nm thick shells, respectively. Really, for the former sample three dynamic modes are registered: the same ultra-fast Arrhenius one ($Q = 60$–70 kJ/mol) and the modes with anomalously high apparent activation energies: $Q = 400$ and 560 kJ/mol.

The extraordinary multi-modal glass transition dynamics is observed for monomolecular shell of the 20PVP/80SiO2 sample

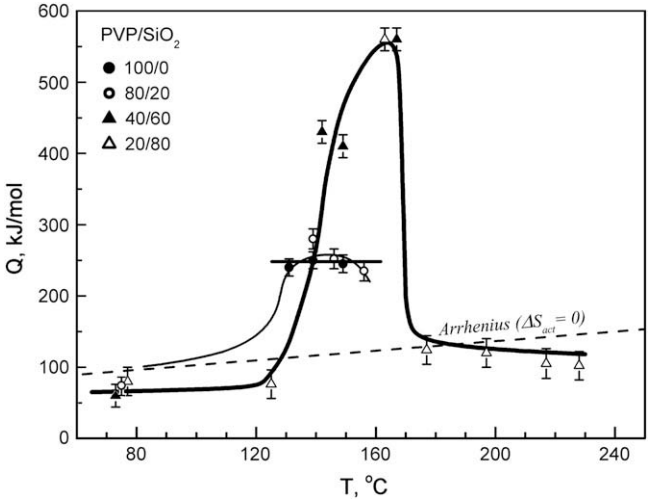

Fig. 14. Dispersions of apparent activation energies *Q* for segmental motion within waterless PVP glass transition as a function of temperature, as determined by DSC for neat PVP and three indicated compositions of PVP/SiO_2 particles.

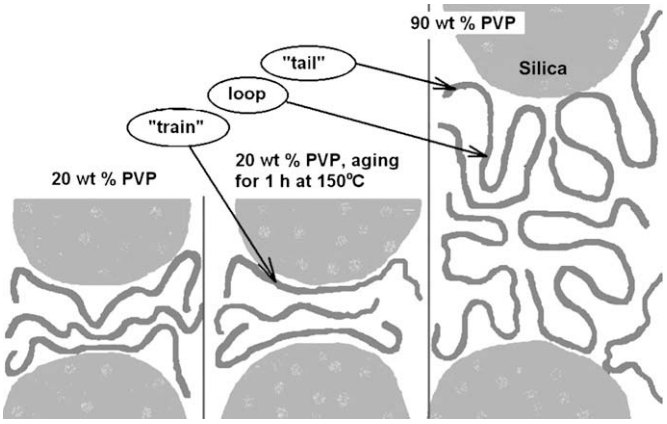

Fig. 15. A scheme of different conformational states of PVP chains in the PVP/silica composites with 20 and 90 wt% PVP.

annealed at 150 °C: it includes ultra-fast dynamics at 75–125 °C ($Q = 80$ kJ/mol) and strongly hindered (ultra-slow) dynamic modes, cooperative ($Q = 560$ kJ/mol, at ~160 °C) and Arrhenius-like ($Q \approx 100$ kJ/mol). Of interest, the latter mode was registered at anomalously high temperatures, from 175° to 230 °C, i.e. in the range of new heat capacity step. Thus, for 1–2 nm thick shell the surprisingly high heterogeneity in the glass transition dynamics was characterized with the co-existence of only three "abnormal" (for glass transition) segmental motions with activation barriers differing almost by one order of magnitude.

Analysis of the multi-modal dynamics observed may be done on the basis of the notions of constrained dynamics; nano-confinement effects, and the common origin of α- and β-relaxations. Of course, the presence of both PVP/silica and PVP/air interfaces, as well as the presence of "train", tail and loop elements in PVP chain conformations (see the scheme in Fig. 15), and the possibility of the long-lived density inhomogeneities in PVP must also be taken into consideration.

Dynamics of surface-bound polymer layer is a function of both the configuration of chains and the proximity of the segments to the surface. Strongly hindered segmental dynamics modes are observed within 1–2 and 2–5 nm thick shells, that is, in adsorbed PVP layers with the thicknesses equal to about one or two Kuhn statistical segment lengths. It is clear that a considerable fraction of segments are tightly-bound, via H- and Lewis bonding, with silica surface as "trains" located in the immediate proximity to silica surface and just corresponding to the dynamically slower PVP moieties. A few adjoining surface-bound "train" segments determine, evidently, the motional unit of hindered cooperative motion at ~160 °C. Restriction of segmental relaxation results also in much slower physical aging processes in 1–2 nm thick shell.

Of special interest are the dynamically slowest segments, for which motion unfreezing is observed at 200–230 °C only but, despite that, their dynamics obeys Arrhenius relation for non-cooperative relaxations. In this case, separately located, extended "train" segments become to be especially strongly attached to silica surface after the treatment at 150 °C that was confirmed by IR data (Figs. 7 and 8).

The opposite effect of accelerating dynamics and the manifestation of ultra-fast segmental dynamics mode at temperatures of 60–80 °C, i.e. approximately in the region of PVP β - relaxation, is totally understandable and may be treated in terms of the experimentally proved notion of the common segmental nature of α - and β - relaxations in flexible-chain polymers (see reviews [33,64,79]). As shown in our studies, these basic relaxation transitions are the intermolecularly cooperative (α) or quasi-independent (β) rotary motions, respectively, of chain sections approximately equal in length to a Kuhn statistical segment (correlation length). At low frequencies, the typical degree of intermolecular motional cooperativity in the glass transition $Z = Q_\alpha/Q_\beta \approx 3-5$ where Q_α and Q_β are the activation energies of the relevant transitions. Chain confinement to nanometer-scale volumes or chain location at free polymer surface, as well as the locally loosened molecular packing, may lead to a partial decreasing or even total collapse of intermolecular motional cooperativity. It is noteworthy that the correlation between the segmental dynamics and the local density in the vicinity of each segment was shown in computer simulations [12].

Therefore, the physical limit for "anomalous" decreasing T_g (accelerating glass transition dynamics) is the transformation of cooperative α- transition into non-cooperative, Arrhenius β- transition ($Z \approx 1$). Then, glass transition may be observed in the temperature range of the β - transition, with parameters $T = T_\beta$ and $Q = Q_\beta$. Such "anomalous" lower-temperature displacements of T_g were registered for complex polymer systems [31–35,80–83], for dynamics in nanoconfined geometries [5–7,12,13], or at free polymer surface [4,19].

In the present work, the accelerated dynamics corresponding to the onset of glass transition in PVP shells from ~70 to 80 °C, with the Arrhenius activation energy $Q < 100$ kJ/mol (Fig. 14), is just associated with collapsing motional cooperativity and α–β transformation. For highly-porous core–shell samples with 20 or 40 wt% PVP this may occur at free surface, whereas in the case of non-porous nanocomposites with 80 or 90 wt% PVP this ultra-fast dynamics unfreezes in loosely packed points inside a polymer matrix. In both cases, dynamics of tail and some loop segments may, obviously, be responsible for ultra-fast motion in shell glass transition.

4. Conclusion

In this work, we studied the interfacial interactions and glass transition dynamics at interfaces in a set of the well-defined dried silica core–PVP shell nanoparticles as model "interface-controlled materials". The polymer shell thickness in these particles, obtained via pseudo-liquid state procedure, varied from 1 to 2 nm (monomolecular layer) up to ~10–20 nm (around radius of gyration of macromolecule). Relatively uniform PVP nanoshells could be formed because of the large difference between PVP–PVP and PVP–silica interactions (~7 and 40–50 kJ/mol, respectively) and enhanced PVP diffusive mobility in the pseudo-liquid state.

The comprehensive characterization of the structural organization and geometry of these particles was based on utilizing together such experimental methods as low-temperature nitrogen adsorption (LTNA), quasi-elastic light scattering (QELS), AFM, FT-IR spectroscopy, and densitometry techniques. The new information on the interfacial interactions and glass transition dynamics at interfaces and their interrelationships were obtained using far- and mid-IR spectroscopy and DSC. To our knowledge, far-IR spectroscopy combined with DSC analysis of the dispersion of activation barriers to segmental motion within the glass transition were applied to nanoscale polymer layers for the first time in this work.

Far- and mid-IR spectra revealed the strong PVP–silica interactions of two kinds: hydrogen (H-) bonding and "soft" Lewis acid–base interactions. These interactions were maximal for 1–2 nm thick monomolecular PVP shell (20 wt% PVP in core–shell particle) annealed at 150 °C, obviously, due to the presence of the most content of "trains" of chain segments interacting with silica surface. Such interactions were responsible for the irreversible character of adsorption of PVP monolayer. Some changes in dynamics and conformational state, caused by the transformation of bulk PVP into

nano-dispersive state, were also confirmed by the far-IR spectra (20–500 cm^{-1}).

"Anomalous" and quite different, multi-modal segmental dynamics was revealed by DSC in the glass transition of PVP shells, as a consequence of the PVP–silica interfacial interactions and the presence of PVP–air interfaces. The distinct correlations between dynamics and interfacial interactions were found. Unlike "normal" cooperative dynamics in the narrow glass transition of neat PVP (apparent activation energy $Q = 250$ kJ/mol), we observed multi-fold broadening, to lower and higher temperatures, and two-stage character of glass transition for PVP shells; additionally, the wide Q dispersions within transition range were observed. The behavior of 1–2 nm thick PVP monolayer was of special interest. In this case, glass transition could cover the temperature range between 70 and 230 °C, and the "normal" physical aging process (enthalpy changes after thermal treatment) was suppressed. Moreover, Q value varied from 80 to 560 kJ/mol; this dispersion included the contributions of constrained cooperative and non-cooperative dynamic modes, as well as ultra-fast, Arrhenius-like mode to the glass transition. The cooperative dynamics mode, peculiar typically to block PVP, was absent at all in the glass transition of adsorbed PVP monolayer.

The ultra-fast dynamic mode (at ~70–80° C) in the glass transitions of PVP shells could be treated in terms of the notion of the common nature of α - and β - relaxations and collapsing motional cooperativity in molecular tails, or some of loop segments at free surface and in loosely packed points of PVP.

The direct correlations observed between the interfacial interactions, conformation state of macromolecules at interfaces and peculiar glass transition dynamics within interfacial polymer monolayer are of significance for the development of high performance polymer nanocomposites, adhesives, coatings, or inorganic core–polymer shell nanoparticles.

References

[1] Jackson CL, McKenna GB. J Non-Cryst Solids 1991;131–133:221.
[2] Keddie JL, Jones RAL, Corey RA. Europhys Lett 1994;27:59.
[3] Wallace WE, van Zanten JH, Wu WL. Phys Rev E 1995;52:R3329.
[4] Forrest JA, Dalnoki-Verres K, Stevens JR, Dutcher JR. Phys Rev Lett 1996;77:2002.
[5] Huwe A, Kremer F, Behrens P, Schweiger W. Phys Rev Lett 1999;82:2338.
[6] Giannelis EP, Krishnamoorti R, Manias E. Adv Polym Sci 1999;138:107.
[7] Anastaisiadis SH, Karatasos K, Viachos G, Manias E, Giannelis EP. Phys Rev Lett 2000;84:915.
[8] Vaia RA, Giannelis EP. MRS Bull 2001;26:394.
[9] Tien YI, Wei KH. J Appl Polym Sci 2002;86:1741.
[10] Schonhals A, Goering H, Schick CH. J Non-Cryst Solids 2002;305:140.
[11] Kuppa V, Manias E. J Chem Phys 2003;118:3421.
[12] Manias E, Kuppa V. Eur Polym J 2002;8:193.
[13] Zax DB, Yang DK, Santos RA, Hegemann H, Giannelis EP, Manias E. J Chem Phys 2000;112:2945.
[14] Kuppa V, Foley TMD, Manias E. Eur Phys J E 2003;12:159.
[15] Lu H, Nutt S. Macromolecules 2003;36:4010.
[16] Ellison CJ, Torkelson JM. Nat Mater 2003;2:695.
[17] De Gennes PG. Eur Phys J E 2000;2:201.
[18] Alcoutlabi M, McKenna GB. J Phys Condens Matter 2005;17:R461.
[19] Forrest JA, Dalnoki-Verres K. Adv Colloid Interface Sci 2001;94:161.
[20] Hrobaricova J, Robert JL, Calberg C, Jerome R, Grandjean J. Langmuir 2004; 20:9828.
[21] Urbanczyk L, Hrobaricova J, Calberg C, Jerome R, Grandjean J. Langmuir 2006;22:4818.
[22] Xiong J, Zheng Z, Jiang H, Ye S, Wang X. Composites Part A 2007;38:132.
[23] Rittigstein P, Priestley RD, Broadbelt LJ, Torkelson JM. Nat Mater 2007;6:278.
[24] Blum FD, Young EN, Smith G, Sitton OC. Langmuir 2006;22:4741.
[25] Metin B, Blum FD. J Chem Phys 2006;125:054707.
[26] Vignaud G, Bardeau JF, Gibaud A, Grohens Y. Langmuir 2005;21:8601.
[27] Tsagaropoulos G, Eisenberg A. Macromolecules 1995;28:396.
[28] Bershtein VA, Egorova LM, Yakushev PN, Pissis P, Sysel P, Brozova L. J Polym Sci Part B Polym Phys 2002;40:1056.
[29] Arrighi V, McEwen IJ, Qian H, Serrano Prieto MB. Polymer 2003;44:6259.
[30] Fradiadakis D, Pissis P, Bokobza L. Polymer 2005;46:6001.
[31] Bershtein VA, Levin VY, Egorova LM, Egorov VM, Zhdanov AA, Slonimsky GL, et al. Vysokomol Soed A 1987;29:2360.
[32] Bershtein VA, Levin VY, Egorova LM, Egorov VM, Zhdanov AA, Slonimsky GL, et al. Vysokomol Soed A 1987;29:2553.
[33] Bershtein VA, Egorov VM. Differential scanning calorimetry of polymers. Physics, chemistry, analysis, technology. New York: Ellis Horwood; 1994.
[34] Bershtein VA, Egorova LM, Ginsburg LI. Vysokomol Soed A 1987;29:2564.
[35] Bershtein VA, David L, Egorov VM, Pissis P, Sysel P, Yakushev PN. In: Mittal KL, editor. Polyimides and other high temperature polymers, vol. 3. Utrecht-Boston: VSP; 2005.
[36] Milchev A, Binder K. Macromolecules 1996;29:343.
[37] Starr FW, Schroder TB, Glotzer SC. Macromolecules 2002;35:4481.
[38] Desai T, Keblinski P, Kumar SK. Polymer 2007;47:722.
[39] Douglas JF, Schneider HM, Franz P, Lipman R, Granick S. J Phys Condens Matter 1997;9:7699.
[40] Jones RL, Kumar SK, Ho DL, Briber RM, Russel TP. Macromolecules 2001;34:559.
[41] Day JC, Robb ID. Polymer 1980;21:408.
[42] Iler RK. The chemistry of silica. Chichester: Wiley; 1979.
[43] Legrand AP, editor. The surface properties of silicas. New York: Wiley; 1998.
[44] Ray SS, Okamoto M. Prog Polym Sci 2003;28:1539.
[45] Parfitt GD, Rochester CH, editors. Adsorption from solutions at the solid/liquid interface. London: Academic Press; 1983.
[46] Chuiko AA, editor. Medical chemistry and clinical application of silicon dioxide. Kiev: Naukova Dumka; 2003 [in Russian].
[47] Gun'ko VM, Zarko VI, Leboda R, Chibowski E. Adv Colloid Interface Sci 2001;91:1.
[48] Gun'ko VM, Voronin EF, Mironyuk IF, Leboda R, Skubiszewska-Zięba J, et al. Colloids Surf A 2003;218:125.
[49] Zaman AA, Bjelopavlic M, Moudgil BM. J Colloid Interface Sci 2000;226:290.
[50] Bjelopavlic M, Singh PK, El-Shall H, Moudgil BM. J Colloid Interface Sci 2000;226:159.
[51] Adamson AW, Gast AP. Physical chemistry of surface. New York: Wiley; 1997.
[52] Gun'ko VM, Voronin EF, Zarko VI, Goncharuk EV, Turov VV, et al. Colloids Surf A 2004;233:63.
[53] Gun'ko VM, Voronin EF, Nosach LV, Pakhlov EM, Guzenko NV, et al. Adsorp Sci Technol 2006;24:143.
[54] Gun'ko VM, Voronin EF, Nosach LV, Pakhlov EM, Voronina OE, et al. Appl Surf Sci 2006;253:2801.
[55] Nguyen C, Do DD. Langmuir 1999;15:3608.
[56] Gun'ko VM, Zarko VI, Voronin EF, Turov VV, Mironyuk IF, et al. Langmuir 2002;18:581.
[57] Gun'ko VM, Mikhalovsky SV. Carbon 2004;42:843.
[58] Gun'ko VM. Theor Exp Chem 2000;36:319.
[59] Gun'ko VM, Turov VV, Leboda R, Zarko VI, Skubiszewska-Zięba J, Charmas B. Langmuir 2007;23:3184.
[60] Moynihan CT, Easteal AJ, DeBolt MA. J Am Ceram Soc 1976;59:12.
[61] Lebedeva TL, Fel'dshtein MM, Kuptsov SA, Platé NA. Polym Sci A 2000; 42:989.
[62] Kirsh YE. Water-soluble poly-*N*-vinylamides. Chichester: Wiley; 1998.
[63] Bershtein VA, Ryzhov VA. J Macromol Sci Phys B 1984;23:271.
[64] Bershtein VA, Ryzhov VA. Adv Polym Sci 1994;114:43.
[65] Belopolskaya TV. Dokl Acad Nauk SSSR 1968;180:1388.
[66] Da Costa VM, Fiske TG, Coleman LB. J Chem Phys 1994;101:2746.
[67] Mittal KL, editor. Acid–base interactions: relevance to adhesion science and technology, vol. 2. Utrecht: VSP; 2000.
[68] Chehimi M, Cabet-Deliry E, Azioune A, Abel ML. Macromol Symp 2002; 178:169.
[69] Shi B, Zhang Q, Jia L, Liu Y, Li L. J Chromatogr A 2007;1149:390.
[70] Brogly M, Grohens Y, Labbe C, Schultz J. Int J Adhes Adhes 1997;17:257.
[71] Hamieh T, Rezzaki M, Schultz J. J Colloids Surf A 2001;189:279.
[72] Pattanaik M, Bhaumik SK. Mater Lett 2000;44:352.
[73] Huang CF, Kuo SW, Lin FJ, Wang CF, Hung CJ, Chang FC. Polymer 2006;47:7060.
[74] Morrow BA, Cody IA. J Phys Chem 1976;80:1995.
[75] Granqvist B, Sandberg T, Hotokka M. J Colloid Interface Sci 2007;310:369.
[76] Gun'ko VM, Zarko VI, Turov VV, Oranska EV, Goncharuk EV, et al. Powder Technol, in press.
[77] Bershtein VA, Gun'ko VM, Egorova LM, Guzenko N, Pakhlov EM, et al., in preparation.
[78] Priestley RD, Broadbelt LJ, Torkelson JM. Macromolecules 2005;38:654.
[79] Bershtein VA, Egorov VM, Egorova LM, Ryzhov VA. Thermochim Acta 1994;238:41.
[80] Bershtein VA, Egorov VM, Egorova LM, Sysel P, Zgonnik VN. J Non-Cryst Solids 1998;235–237:476.
[81] Karabanova LV, Sergeeva LM, Yakushev PN, Egorova LM, Ryzhov VA, Bershtein VA. J Polym Sci Part B Polym Phys 2007;45:963.
[82] Bershtein VA, Karabanova LV, Sukhanova TE, Yakushev PN, Egorova LM, et al. Polymer 2008;49:836.
[83] Karabanova LV, Bershtein VA, Sukhanova TE, Yakushev PN, Egorova LM, et al. J Polym Sci Part B Polym Phys 2008;46:1696.